Early cytoplasmic uncoating is associated with infectivity of HIV-1

João I. Mamede[a], Gianguido C. Cianci[a], Meegan R. Anderson[a], and Thomas J. Hope[a,1]

[a]Department of Cell and Molecular Biology, Feinberg School of Medicine, Northwestern University, Chicago, IL 60611

Edited by John M. Coffin, Tufts University School of Medicine, Boston, MA, and approved July 14, 2017 (received for review May 5, 2017)

After fusion, HIV delivers its conical capsid into the cytoplasm. To release the contained reverse-transcribing viral genome, the capsid must disassemble in a process termed uncoating. Defining the kinetics, dynamics, and cellular location of uncoating of virions leading to infection has been confounded by defective, noninfectious particles and the stochastic minefield blocking access to host DNA. We used live-cell fluorescent imaging of intravirion fluid phase markers to monitor HIV-1 uncoating at the individual particle level. We find that HIV-1 uncoating of particles leading to infection is a cytoplasmic process that occurs ∼30 min postfusion. Most, but not all, of the capsid protein is rapidly shed in tissue culture and primary target cells, independent of entry pathway. Extended time-lapse imaging with less than one virion per cell allows identification of infected cells by Gag-GFP expression and directly links individual particle behavior to infectivity, providing unprecedented insights into the biology of HIV infection.

HIV-1 early steps | HIV-1 uncoating | live-cell imaging

HIV is the etiological agent of the AIDS pandemic. To infect a target cell, HIV must complete a series of steps initiating with fusion and release into the cytoplasm, followed by reverse transcription, nuclear translocation, and integration into the host chromatin. After cell fusion, HIV delivers its conical core, referred to as the capsid, into the cytoplasm. The capsid, formed by CA protein hexamers and pentamers, contains several viral and host cell proteins as well as the viral genome (1), and is an interesting target for new antiviral therapies. The disassembly of this fullerene cone composed of CA is termed uncoating, and it is critical to infection (2). Determinants in CA have been shown to influence multiple steps of infection, such as nuclear translocation pathway and preference of HIV sites of integration (3–8), and to influence host responses, such as DNA sensing mediated by cyclic GMP-AMP synthase (cGAS) (9, 10).

To date, there are disagreeing models for the timing and cellular location of HIV-1 uncoating (11). An early model advocated for uncoating at viral fusion, based on the inability to detect CA associated with purified reverse transcription complexes (RTCs) or preintegration complexes (PICs) (12–14). The discovery of TRIM5α and TRIM-CypA's ability to target HIV-1 capsids and block HIV-1 infection revealed the persistence of the viral cone in the cytoplasm after fusion (15–23). Another model suggests that CA is not shed from the RTC and that the intact capsid docks at the nuclear pore (3, 5). This possibility is supported by the observation that CA is a viral determinant in several important steps that occur in the nucleus, including nuclear import and integration site selection of the viral genetic material in the host DNA (3–5, 24). A third proposed model is that uncoating takes place in the cytoplasm as the reverse-transcribing viral genome is transported to the nucleus. This model is based on both fluorescence microscopy observations and assays that exploit the impact on infection from modulated TRIM5 susceptibility (25–29). The HIV-1 capsid uncoating dependence on microtubule stability also supports a cytoplasmic uncoating (25, 26, 30–34). Recently, the importance and dependence on CA of most of the early steps of infection have been partially explained by the identification of a small amount of CA that associates with the PIC in the nucleus (35–38). Because of the differences between these models, the kinetics, dynamics, and cellular location of uncoating of infectious HIV-1 particles have remained controversial topics (4, 25–29, 37, 39, 40).

A major hurdle to the clarification of HIV-1 uncoating is that most uncoating assays examine populations of viral particles. These populations include defective or noninfectious virions and stochastic events leading to nonproductive aborted infection, which confounds data interpretation. These assays inevitably average the behavior of different viral particle phenotypes. So far, the field has been unable to differentiate between defective or ineffectual particles with an anomalous behavior and particles that are associated with productive infection of a target cell. In this study, we leverage a live-cell imaging assay to distinguish particles associated with infection and define their associated behavior. We study the behavior of individual labeled viral particles in cell lines, and primary cells that are HIV-1 targets of infection.

Results

Development of a Live-Cell Imaging Fluorescent Microscopy Assay to Measure HIV-1 Capsid Integrity Loss. To observe the state of the integrity of the HIV conical capsid, we use live-cell fluorescent imaging to monitor HIV-1 capsid integrity by tracking single particles that are dual-labeled with Gag-iGFP, a fluid phase marker, and with the viral genome complex labeled by mCherryVpr (25, 41). The loss of capsid integrity is observed as a loss of fluid phase GFP contained within an intact conical capsid. Multiple groups have shown that the generation of HIV-1 particles with a Gag-GFP polyprotein (HIV-iGFP) releases free GFP after proteolytic viral maturation. The liberated GFP then becomes an intravirion fluid phase marker (41–43). We previously demonstrated that a minority subset of the fluid phase GFP is trapped within the capsid structure (42, 44). This minority of fluid phase GFP trapped within capsids allows the prefusion virions to be differentiated from postmembrane fusion intact conical capsids and capsids that have lost their integrity when particles are dual-labeled with a viral genome complex marker,

Significance

After fusion, HIV delivers its capsid formed of CA proteins into the cytoplasm. The regulated disassembly of the capsid (uncoating) is critical to the timely exposure of the viral genome and infection. The timing of this process is controversial. Utilizing an intravirion GFP fluid phase marker with a live-cell imaging approach, where we use less than one virion per cell, we demonstrate that the uncoating of HIV-1 particles is an early cytoplasmic process taking place ∼30 minutes after fusion, and dependent on ongoing reverse transcription. Early uncoating is observed in culture cells, primary T cells, and macrophages with either HIV or pseudotyped envelope. Partial CA retention with the viral complex facilitates late CA functions, including nuclear import and integration site selection.

Author contributions: J.I.M., G.C.C., and T.J.H. designed research; J.I.M. and M.R.A. performed research; J.I.M. and T.J.H. contributed new reagents/analytic tools; J.I.M., G.C.C., and T.J.H. analyzed data; and J.I.M., G.C.C., and T.J.H. wrote the paper.

The authors declare no conflict of interest.

This article is a PNAS Direct Submission.

Freely available online through the PNAS open access option.

[1]To whom correspondence should be addressed. Email: thope@northwestern.edu.

This article contains supporting information online at www.pnas.org/lookup/suppl/doi:10.1073/pnas.1706245114/-/DCSupplemental.

such as mCherryVpr (Fig. 1*A*). The mCherryVpr is an effective tool to track RTCs as they initiate reverse transcription (14, 25). Here, we leverage the ability to detect the stepwise loss of the GFP fluid phase marker to monitor loss of HIV-1 capsid integrity within living cells using time-lapse fluorescent microscopy (Fig. 1*A*).

To determine the timing of HIV-1 capsid integrity loss after virion fusion, we initially used Chinese hamster ovary (CHOpgsa745) cells infected with vesicular stomatitis virus G glycoprotein (VSV-G) pseudotyped HIV-1–iGFP–mCherryVpr particles (Movie S1). This mutant CHO cell line lacks expression of glycosaminoglycans, resulting in high efficiency of particle fusion and cytoplasmic entry upon cellular engagement (16). The analysis of a well-characterized preparation of virions (Fig. S1) that entered imaged cells reveals that the majority of viral particles show a dramatic loss of most of their GFP, consistent with fusion within an endosome within ∼30 min of cell engagement (Fig. 1 *A* and *B*). This considerable GFP loss is concurrent with fusion, as revealed by using viral particles with S15-tdTomato–labeled membranes (Movie S2). However, as anticipated, a majority of the cytoplasmic viral complexes retain a subset of the GFP trapped within the intact cone. The level of residual GFP is lost from the mCherryVpr RTC marker ∼30 min after fusion, revealing a dual-step loss of GFP from the viral complex.

While this dual-step GFP loss represents the most common phenotype, other viral behaviors are present (Figs. 1*D* and 2*A*). Some particles lose their entire GFP signal after fusion, likely due to incomplete formation of a mature and intact capsid (42). A notable minority population appears to fuse but does not lose the totality of its GFP signal before the end of the data acquisition period (>120 min). We fit the GFP signal with a heuristic double-sigmoid equation (Fig. S2 *B* and *C*) to determine Δt: the time between the first drop in intensity (indicating fusion) and the subsequent loss of the remaining GFP (indicating capsid integrity loss). We find a median postfusion capsid integrity loss of Δt = 25.0 ± 7.3 min (Fig. 1*D*).

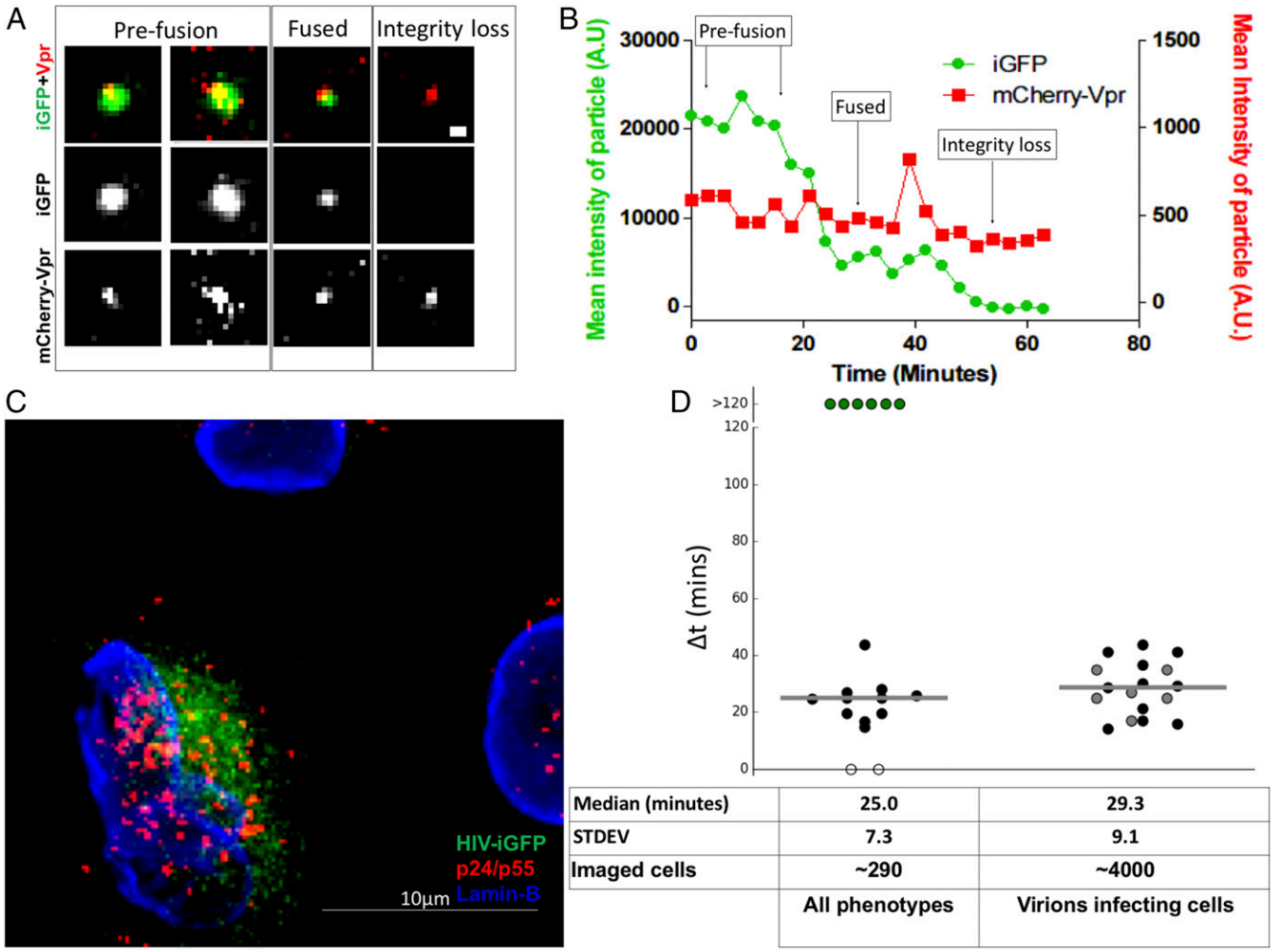

Median (minutes)	25.0	29.3
STDEV	7.3	9.1
Imaged cells	~290	~4000
	All phenotypes	Virions infecting cells

Fig. 1. Live-cell imaging of HIV-iGFP reveals an early timing to capsid integrity loss associated with infection. (*A*) Time course of HIV-iGFP-mCherryVpr infection reveals two independent GFP signal drops leading to complete loss of signal; the mCherryVpr signal is used to track HIV particles. A particle interacts with a target cell; when fusion occurs, there is a first drop of the GFP signal; and when the capsid integrity is compromised, there is a complete loss of the GFP signal. (Scale bar: 500 nm.) (*B*) Time-lapse quantification of mean particle intensity of GFP signal (green) and mCherryVpr (red). (*C*) Cells from a live imaging experiment over 22 h were fixed and stained for p24/p55 (red) and Lamin-B (blue), and de novo signal of HIV-iGFP was also acquired (green). A single particle was able to fuse to this cell, demonstrating a dual-drop phenotype, as shown in Movie S1. (Scale bar: 10 μm.) (*D*) Median time of capsid integrity loss is 25.0 min for dual-drop events: kinetics of iGFP-mCherryVpr particles that undergo total loss of GFP signal Δ(time of total integrity loss − time of fusion) (∼290 cells). Particles that lost all GFP simultaneously to fusion were given a value of 0 (white circles), particles that kept GFP until the end of the time lapse were given a value of 120 min (green circles), particles that had two signal drops were given a value of Δ(time of total integrity loss − time of fusion) obtained with data fitting and were dual-labeled with mCherryVpr (black circles), and particles with two iGFP signal drops without mCherryVpr marker are shown as gray circles. (*D*, *Right*) Median time of capsid integrity loss is 29.3 min for cells that became infected, only infected cells that presented one virus phenotype were plotted, and all cells that became infected had a dual-drop HIV-iGFP phenotype (∼4,000 cells). Medians are shown as gray horizontal bars. STDEV, standard deviation.

In complementary experiments, we labeled HIV-iGFP viruses with an Integrase (IN)-mRuby fusion protein that has been shown to remain with the PIC after entry into the nucleus (30, 36). We used this alternative marker for the RTC/PIC and measured approximately the same timing of integrity loss as when using mCherryVpr as an RTC marker, 23.6 ± 8.0 min after fusion (Fig. 2*A* and Movie S3). These results provided validation for the ability to measure capsid integrity loss of the cytoplasmic HIV complex containing the viral genome.

Phenotypical Differentiation of Virions Associated with Infectious Events. To understand the biological consequences of HIV-1 uncoating, it is critical to directly connect either the dual-step drop or stable cone integrity phenotype to infection. To tie infectivity to individual virion behavior, we developed an extended time-lapse imaging approach. We follow multiple fields of the CHOpgsa745 cells for ∼2 h, capturing a two-color z-series every 4.5 min. After this initial period, we imaged with an increasing time lapse extending up to every 30 min for the next 24–42 h. Because the HIV-iGFP construct contains a Gag-GFP fusion, any infected cell that is producing new viruses is readily identified by its de novo Gag-GFP expression and new virion assembly (Fig. 1 *C* and *D*). These studies were done under conditions of very low virus concentrations, where there is typically less than one virion per cell. This allows the ability to directly connect individual particle capsid integrity behavior to infection. Examining ∼4,000 cells in this manner led to the identification of 21 infected cells. As expected, only cells that were shown to be associated with a GFP-labeled particle later became infected, as demonstrated by the expression of the iGFP-Gag fusion protein. Analysis of the behavior of viral particles that fused with the infected cells showed that 17 of these cells interacted with a single virion. Eleven of these cells interacted with a dual-labeled particle (black solid dots in Fig. 1*D* and Movie S4), while six cells were infected by particles that were labeled with HIV-iGFP but not mCherryVpr (gray solid dots in Fig. 1*D* and Movie S4). In all 11 dual-labeled cases, the infectious event is associated with a single virion that lost its capsid iGFP signal within 45 min after fusion. The Δt measured by GFP intensity is presented in Fig. 1*D*, with a median of 28.7 ± 9.1 min. This occurred in the cytoplasm for all observed virions that went on to infect the cells. This observation demonstrates that only the early loss of cone integrity ∼30 min postfusion is followed by infection. The remaining four infected cells that interacted with more than one fused viral particle are not shown in Fig. 1*D*. Within each of these latter four cells, we observed the presence of a particle with a dual-step loss of GFP.

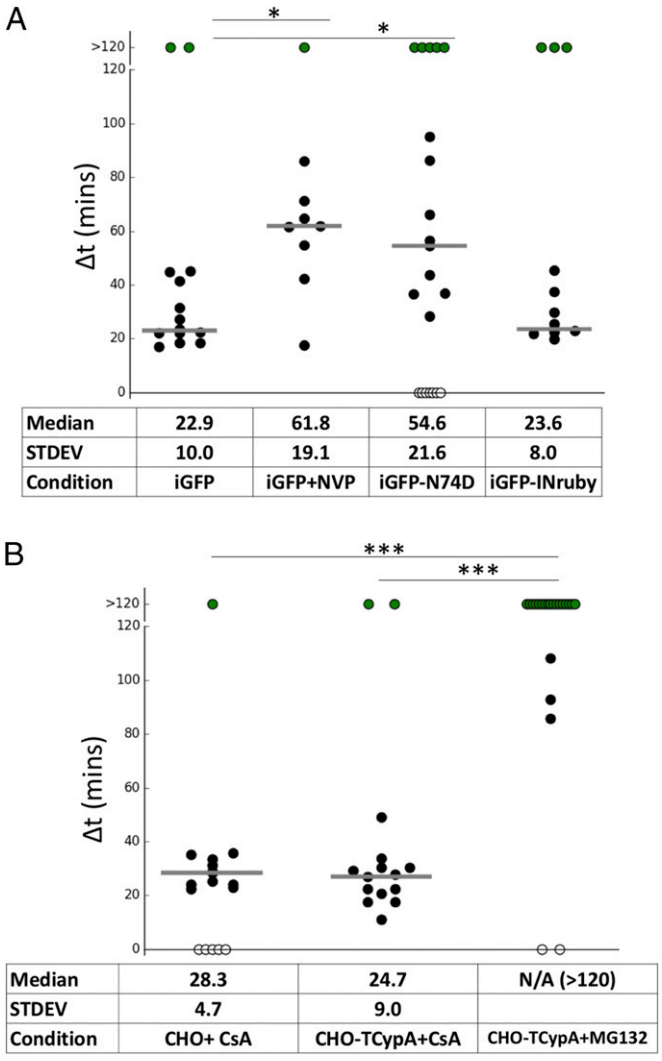

Fig. 2. Modulation of HIV-iGFP capsid integrity loss. (*A*) NH4Cl-synchronized infection with either WT or N74D capsid and with NVP washout 50 min postfusion. The capsid integrity loss was delayed until NVP removal. N74D capsid integrity loss is ∼30 min slower compared with WT, and HIV-iGFP viruses labeled with IN-Ruby behave like mCherryVpr particles. (*B*) NH_4Cl-synchronized infection of CHO or CHO-TRIMCypA cells has a normal phenotype in the presence of CsA, and viral capsid integrity was maintained in TRIM bodies in the presence of MG132. STDEV, standard deviation. *$P < 0.5$; ***$P < 0.01$.

Modulation of Viral Capsid Integrity. Building on the correlation of early capsid integrity loss with virion infectivity, we extended our studies to evaluate the potential impact of conditions previously suggested to alter the timing of uncoating to determine if they modulated the time between fusion and cone integrity loss (Δt) on our findings. To establish a parallel between a previous assay that indirectly examines HIV-1 uncoating and infection with HIV-iGFP (28, 39, 45), we performed a CsA washout assay that verified a similar timing of capsid integrity loss as observed by the imaging assay. The CsA washout assay showed an integrity loss at 28 min (50% of GFP^+ cells) in CHOpgsa745 cells that were stably expressing TRIM-CypA (Fig. S2*A*). As we previously showed with the CsA washout (28), delaying reverse transcription with the transient presence of nevirapine (NVP) pauses capsid integrity loss until NVP removal from the media (Fig. 2*A* and Movie S5). The insertion of an N74D mutation into the HIV-iGFP CA causes a delay in integrity loss, a finding also coincident with previous indirect studies (28) (Fig. 2*A*). In another approach to evaluate the live-imaging assay's ability to correctly measure the integrity of HIV-iGFP capsid, we measured the impact on capsid integrity by modulating TRIM-CypA restriction. Typical TRIM-CypA restriction is demonstrated by a quick destruction of HIV-iGFP particles after fusion (Fig. S3*B*) that is not present after proteasome function is inhibited with MG132 (46). Preventing TRIM-CypA restriction with CsA shows normal capsid integrity loss progression, while the incubation with MG132 blocks the loss of HIV-1 viral capsid integrity by capturing intact viral capsids in TRIM-CypA bodies (44) (Fig. 2*B* and Movie S6).

Inhibiting First-Strand Transfer of Reverse Transcription by Reversibly Inhibiting RNase H Delays Capsid Integrity Loss. After observing that integrity loss of the capsid happens ∼30 min after fusion and is dependent on the ability of HIV-1 to perform reverse transcription, we explored the impact of the first steps of early reverse transcription product formation on the loss of capsid integrity. An emerging hypothesis to the link between early reverse transcription products and the loss of capsid integrity has been recently backed by a study based on both theoretical and mutational studies. Cosnefroy et al. (29) suggested that the first-strand transfer of reverse transcription might play a crucial role in core disassembly. However, another concurrent report that measured the binding of tetrameric CypA to the capsid as a tool to follow

CA pointed to no correlation between first-strand transfer and uncoating (27). This study used a reverse transcription RnaseH–deficient mutant with no visible impact over time on the levels of CypA binding to the capsid compared with WT (27). Using an RnaseH inhibitor specific to HIV-1 reverse transcription (7390; shown as 8b in ref. 47), we can block the first-strand transfer of reverse transcription while allowing reverse transcription activity (Fig. S4). Using the CsA washout assay, we observe that the removal of the RnaseH inhibitor 105 min after fusion allows restoration of a normal course of infection (Fig. 3*A*). The direct measurement of the integrity of individual capsid cores in the presence of RnaseH inhibitor showed a delay on capsid integrity loss. When the inhibitor 7390 was removed, capsid integrity loss was rapidly observed (Fig. 3). This finding supports the model that changes in HIV-1 capsid integrity are influenced by the occurrence of first-strand transfer of the reverse transcription process within an intact capsid core.

Early Capsid Integrity Loss Is Observed in Primary Blood Cells. An advantage of our live-cell imaging assay is that it can be applied to different cell types and viral tropisms. To extend our studies to more biologically relevant cell types, we infected CD3/CD28-activated $CD4^+$ T cells with replication-competent, CXCR4-tropic HIV–iGFP–NL4-3 labeled with mCherryVpr. Here, our live-imaging assay yields a median postfusion capsid integrity loss of $\Delta t = 22.8 \pm 8.5$ min (Fig. 4 and Movie S7). This result is consistent with the early capsid integrity loss of $\Delta t = 28.7 \pm 9.1$ min observed in CHOpgsa745 cells challenged with VSV-G pseudotyped viruses associated with infection (Fig. 1*D* and Movie S4). Infection of monocyte-derived macrophages (MDMs) with VSV-G HIV-iGFP shows integrity loss with an average $\Delta t = 17.2 \pm 7.2$ min (Fig. 4). Infection in MDMs might be expected to result in a slower capsid integrity loss since it has been reported that macrophages have relatively low dNTP concentrations (40, 48, 49) and delayed completion of reverse transcription (28). However, the imaging assay has suggested that capsid integrity loss is associated with early reverse transcription, which might be less sensitive to dNTP concentrations (29, 50). Consistent with this interpretation, we show that the timing of capsid integrity loss in macrophages can be modulated by transitory NVP treatment (Fig. 4). The clear delay of capsid integrity loss upon NVP treatment is present both in primary and tissue culture cell lines, and therefore supports the concept that HIV capsid integrity loss does not require the completion of reverse transcription, but is influenced by the early steps of provirus generation, to result in a successful infection.

Capsid Integrity Loss Happens Simultaneously with CA Shedding. These data demonstrate a loss of capsid integrity in infectious particles, as measured by total GFP loss from the viral capsid. However, monitoring capsid integrity cannot differentiate between leaking through a small hole in the capsid cone or a catastrophic loss of a majority of CA from the RTC. Historically, uncoating is defined as a loss of the CA that forms the cone structure. However, it is not anticipated that this loss is complete since a small amount of CA has been shown to play a role in viral trafficking, microtubule association, nuclear pore translocation, and preferential site of integration, and it has more recently been associated with HIV nuclear complexes (35–37). It is therefore crucial to assess the level of CA when the cone integrity is changing. To directly quantitate the loss of CA and compare it with capsid integrity loss, we used time-lapse fluorescent imaging, followed by correlative fixed immunofluorescence structured illumination microscopy (3D-SIM). We performed our HIV-iGFP live-imaging capsid integrity assay and fixed the samples 40 min after NH_4Cl-synchronized fusion. At this time point, we anticipated that approximately half of the cores would remain intact. The samples were permeabilized and stained for CA, with DAPI counterstain.

In Fig. 5*A*, we show anti-CA antibody staining of a representative particle that was observed to undergo a dual drop of GFP intensity (Movie S8). Measurement of CA levels of individual particles that are intact, are fused, or have entered a cell and then

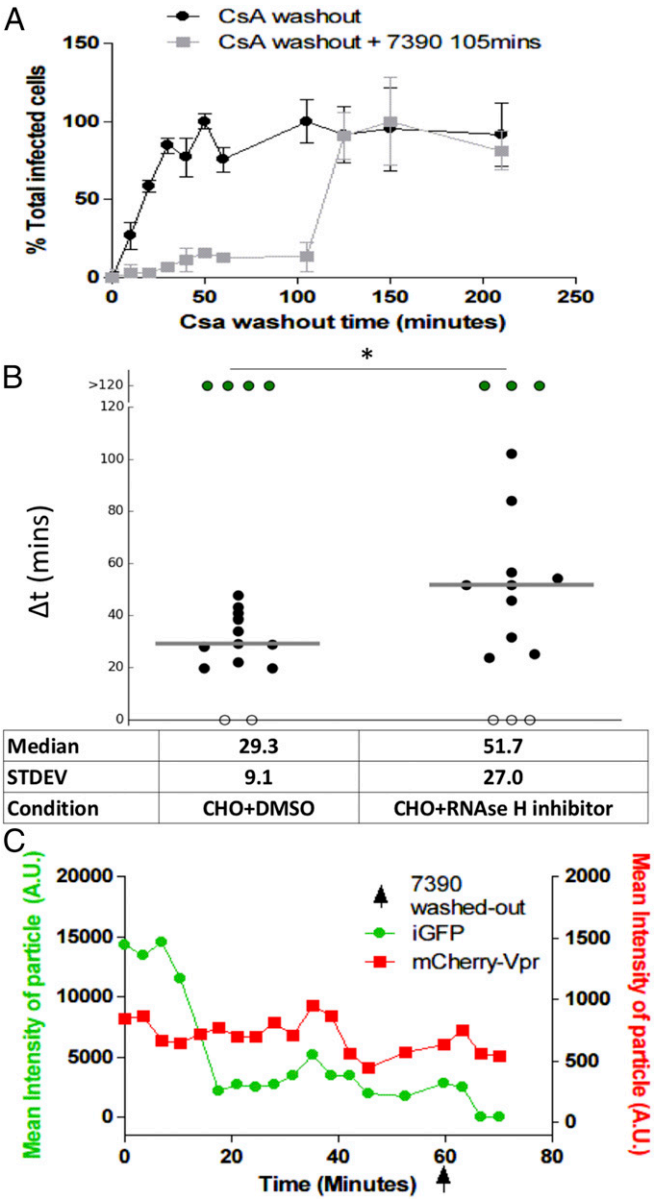

Fig. 3. Transient inhibition of reverse transcription RNAseH activity results in a delay of capsid integrity loss. (*A*) CsA washout of CHO-TRIMCypA cells in the absence of 7390 (black) and with 7390 washed out for all wells at 105 min (gray). (*B*) Δt for infection of CHO cells incubated and washed with DMSO mock (*Left*) and 7390 (*Right*); the capsid integrity loss was delayed in accordance with 7390 removal (50 min postaverage fusion of all particles). Medians are shown as gray horizontal bars. (*C*) Mean particle intensity of GFP signal (green) and mCherryVpr (red) in the presence of 7390, followed by its washout (arrow) 50 min postfusion. STDEV, standard deviation. *$P < 0.5$.

lost capsid integrity shows statistically significantly lower levels of CA associated with the viral complex (Fig. 5 *B* and *C*). These observations effectively and crucially link the step of capsid integrity loss measured by complete loss of fluid phase GFP to the loss of most of the CA from the complex. This loss of the majority of CA under the current experimental conditions is likely a consequence of the disassembly of much of the cone (i.e., uncoating). By measuring the distances to the plasma membrane and nuclear membranes with a previously described method (25), we determine that all the uncoated viral complexes are located in the cytoplasm. We do not observe any viral complexes in nuclei at the moment of cone integrity loss. These findings are consistent with

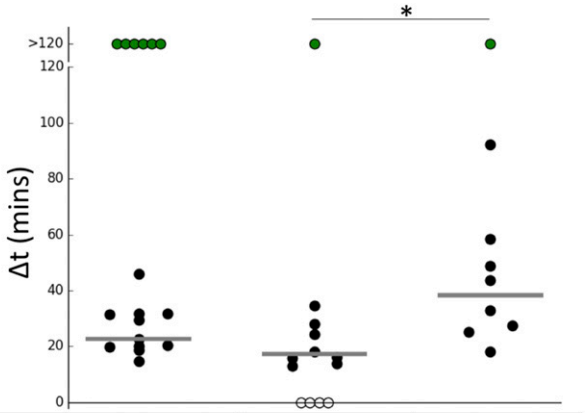

Median	22.7	17.2	38.2
STDEV	8.5	7.2	22.3
Condition	CD4 T-cell	MDM	MDM+NVP wash

Fig. 4. Early capsid integrity loss is observed in primary HIV target cells. Infection of $CD4^+$ T cells (WTEnv) and macrophages (VSV-G pseudotypes) resulted in a similar timing of capsid integrity loss. Uncoating in macrophages was delayed by NVP washout (washed 40 min postaverage fusion). Medians are shown as gray horizontal bars. STDEV, standard deviation. *$P < 0.5$.

capsid uncoating in the cytoplasm in accordance with findings linking microtubule dependence on uncoating (25, 26, 30–34) (Fig. 5 *A* and *C*).

To provide additional kinetic insight, and further technical validation, where antibody binding will not be a factor of staining or temporal detection, we used particles with a tetracysteine motif inserted in *CA* and directly labeled with ReAsH (46). Labeling with CA-ReAsH, together with iRFP670-Vpr incorporation into HIV-iGFP, generates triple-labeled particles, allowing the simultaneous detection of changes in both GFP and CA (Movie S9). The complete loss of GFP from the capsid and loss of the ability to detect CA-ReAsH signal happen quasi-simultaneously, and are well correlated in time ($R_{spearman} = 0.62$) (Fig. 5*D*). Although the CA-ReAsH signal suffers a big drop in signal concurrently with capsid integrity loss and appears to be completely lost during the live-imaging acquisition, fixation and CA staining 45 min postfusion show small amounts of CA-ReAsH that are associated with the complex (Fig. 5*E*). The small amount of ReAsH signal cannot be efficiently detected in the less optimal conditions of live-cell imaging, but are readily detectable in the more optimal conditions of fixed-cell imaging. To ascertain that the CA-ReAsH signal loss is not due to photobleaching, we applied our analysis to viruses that did not fuse, but were on the glass coverslip or on cell membranes in the same live-cell imaging experiments (Fig. S5). These unfused viruses were photostable well beyond the typical uncoating times. We also performed photobleaching control analysis on several thousand virions that were spun onto glass and then imaged with the same experimental conditions as the live-cell imaging experiments (Fig. S6 and *SI Text*). We find that photobleaching is a smooth monotonic process which cannot be the cause of the abrupt CA-ReAsH signal loss we observe during uncoating.

Together, two different approaches, correlative quantification of immunostained CA levels in fixed cells and live-cell imaging of ReAsH-labeled CA, allowed the direct measurement of CA levels within the viral complexes. Both approaches show a correlation between the loss of iGFP and a substantial, but partial, loss of CA.

CA Shedding Is an Early Cytoplasmic Event in Primary Cells. To determine if uncoating kinetics were similar in the more biologically relevant context of the infection of primary T cells with an HIV envelope, we performed live-cell imaging experiments with replicative HIV-iGFP with WTEnv (pNL4-3) followed by fixation at 1 h after viral challenge with unsynchronized entry. The infected cells were then counterstained with DAPI and mAbs to p24. Quantification of p24 levels in the three different populations (unfused particles, fused particles with intact cores, and complexes where core integrity is lost) shows distinct levels of p24 associated with each population. This analysis reveals the capsid integrity loss is coincidental with a statistically significant loss in CA that happens early after fusion and is a cytoplasmic process (Fig. 6 *A* and *B*) in activated primary CD4 T cells. The levels of p24 in the three populations defined by the GFP fluid phase marker in the primary CD4 T cells infected with an HIV envelope (Fig. 6*C*) are similar to those observed during infection of the CHO cells in an analogous experiment (Fig. 5*B*).

We also performed complementary experiments where we infected MDMs with VSV-G pseudotyped HIV-iGFP that was double-labeled with IN-mRuby in the presence of Vpx virus-like particles (VLPs). The fusion was synchronized by the presence of NH_4Cl in the media. After starting the live-cell imaging, we allowed fusion to occur by removing the NH_4Cl in the system and fixed the sample ∼50 min after fusion. Although macrophages showed a high particle deletion rate, as observed by the disappearance of several particles that fused into the cell in comparison to cell lines or primary CD4 T cells, it was possible to capture representative events of IN-mRuby–labeled particles that were unfused or fused and particles where the capsid integrity was lost. Using the same CA staining conditions as for the CD4 T cells, it was again observed within this small dataset that the complete loss of GFP also results in a reduction of the amount of CA in the particles (Fig. 6 *A*, *C*, and *D* and Movie S10).

Together, these experiments performed in primary cells that are the natural targets of HIV show that HIV-1 uncoating occurs at the moment of capsid integrity loss, which is also indicated by iGFP loss from particles in the cytoplasm.

Discussion

In this study, we followed HIV-1 uncoating using a live-imaging approach where we can analyze one viral particle per cell and directly connect the behavior of that particle to infection, as revealed by the expression of the GFP-tagged Gag polyprotein after integration. Most of what is currently known about HIV-1 uncoating has come from in vitro biochemical approaches, mutation-based methods, and indirect observations that result from cellular mechanisms of viral restriction. The approaches related to restriction were limited by a lack of demonstration that the loss of sensitivity to restriction was a consequence of uncoating. In contrast, in situ imaging of fixed or live cells was able to show changes in CA amounts in postfusion particles (26–28, 36). Unfortunately, these methods provided minimal kinetic information and no ability to determine which behaviors of individual particles led to a successful infection. This is because, typically, most of the HIV viral complexes within a cell are not able to infect a cell (51). In some cases, this is likely due to defects in the particle. However, the virus also faces a minefield of stochastic events where restriction factors and innate antiviral responses, correctly completing reverse transcription, nuclear translocation, and correct integration while avoiding recombination and autointegration, stand as obstacles to infection even though the viral function is normal. For example, only one-third of the reverse-transcribed viral genomes that reach the nucleus go on to integrate as required for productive infection (52). This is a high rate of attrition that can be a consequence of stochastic events rather than genetic defects (51). The only way to account for such stochastic events is direct observation of individual particles.

The live-cell imaging method that was used in this study allowed the ability to connect the detailed behavior of HIV-1 particles to cell infection. In this study, we show that the HIV-1 core loses its integrity and a majority of its CA protein ∼30 min after being released into the cytoplasm after fusion. Uncoating of all observed particles that go on to infect a cell is completed by 45 min after fusion. By using a "one-particle, one-cell" approach, it was possible to follow the actual fate of capsid, specifically in HIV-1 particles

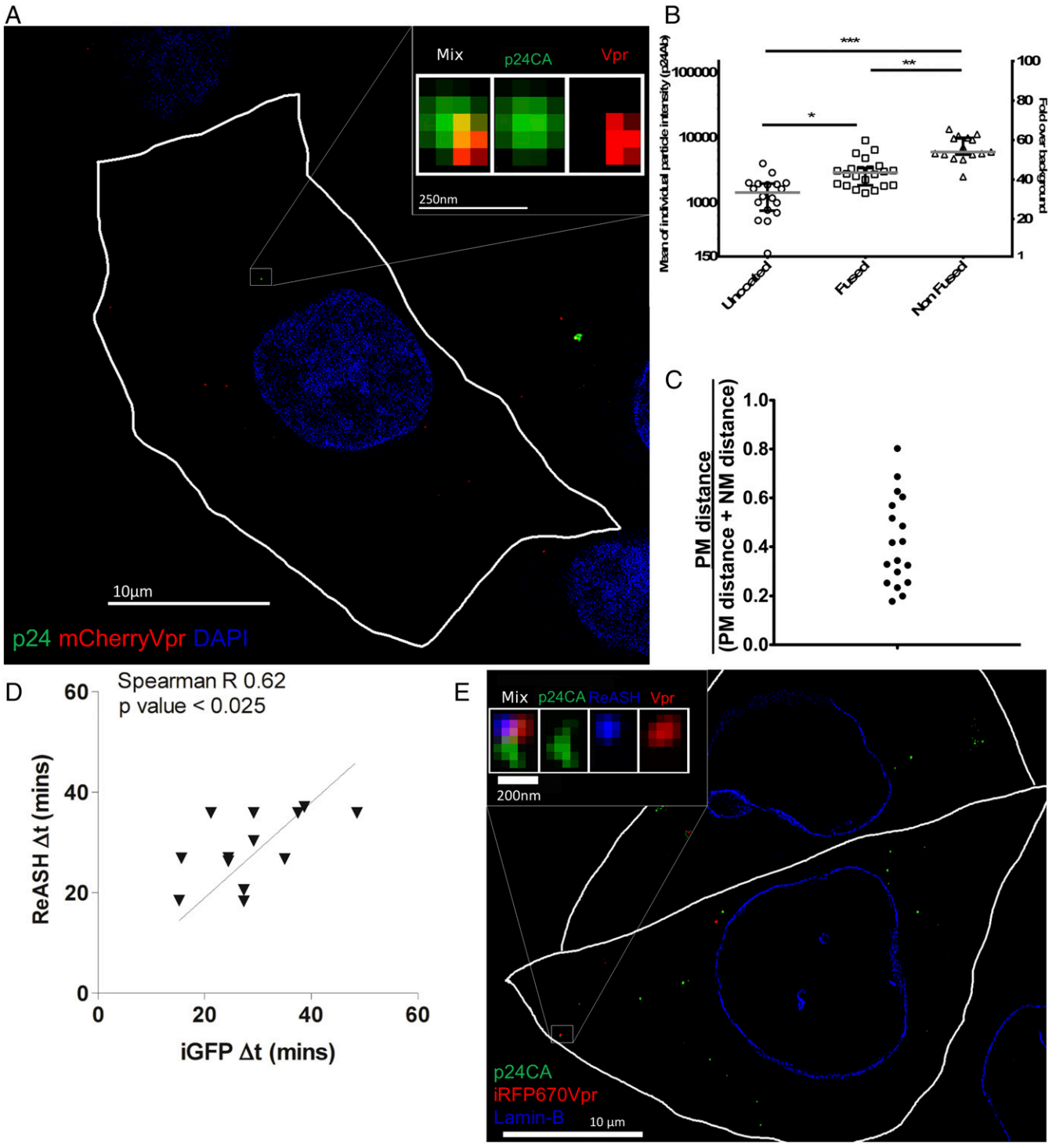

Fig. 5. Quantification of CA in viral complexes links capsid integrity loss to uncoating. (*A*) Three-dimensional SIM superresolution imaging of cells fixed after live imaging for 40 min. (Scale bar: 10 µm.) (*Inset*) Particle that showed two drops and complete GFP signal loss shows a positive signal for CA (green) and Vpr (red), using nuclear staining with DAPI (blue). (Scale bar: 250 nm.) (*B*) Mean intensity and signal-to-noise ratio of all live-imaged individual particles. Groups were defined by their live-imaging GFP capsid integrity phenotype. Medians of the individual events are represented by the gray bars, and interquartile ranges are shown as error bars. (*C*) Particles with a complete loss of capsid integrity locate in the cytoplasm after measurement of the distance from the particle to plasma and nuclear membranes [value of 1 means nuclear membrane location, value of 0 means located at the plasma membrane (PM)]. (*D*) HIV-iGFP-ReAsH-iRFP670Vpr particles were plotted by timing of complete loss of GFP (*x* axis) and timing of complete loss of ReAsH signal (*y* axis). (*E*) Three-dimensional SIM superresolution imaging of cells that were fixed after live imaging for 45 min: p24 (green), Lamin-B (blue), and iRFP670Vpr (red). (Scale bar, 10 µm.) (*Inset*) Magnification represents a particle where two intensity drops were observed, resulting in a complete loss of GFP signal. An uncoated particle fixed after live imaging that is positive for p24 (green), CA-ReAsH (blue), and iRFP670Vpr (red) is shown (Scale bar: 200 nm.) $*P < 0.5$; $**P < 0.1$; $***P < 0.01$.

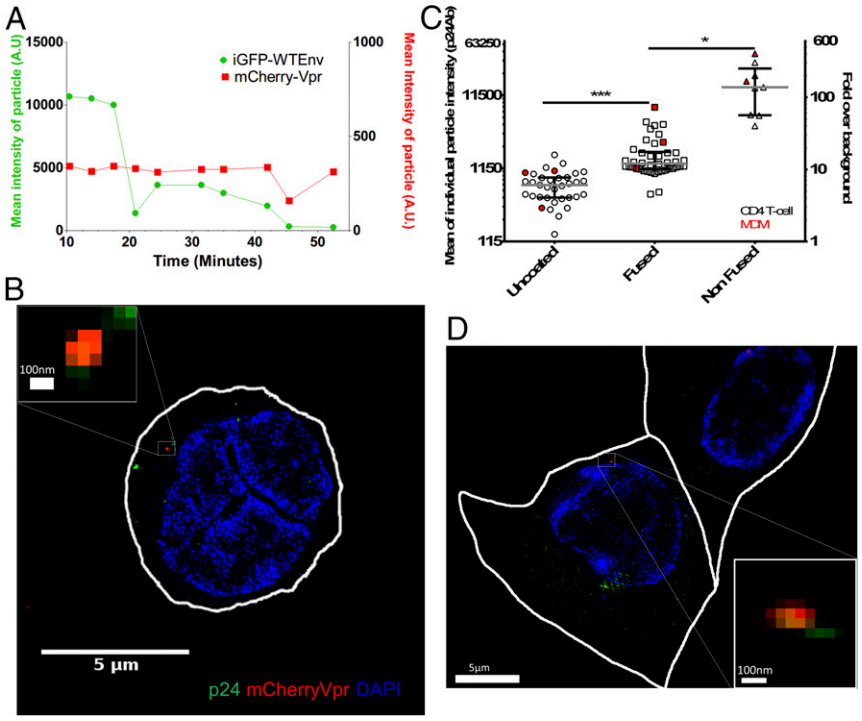

Fig. 6. Quantification of CA in viral complexes in primary cells shows a loss of CA after capsid integrity loss. (*A*) Mean particle intensity of GFP signal (green) and mCherryVpr (red) of an individually tracked, dual-labeled HIV-1 particle; the sample was fixed at 55 min and represents the same event as in *B*. (*B*) Three-dimensional SIM superresolution imaging of a CD4 T cell fixed after live imaging for 55 min. (Scale bar: 5 µm.) (*Inset*) Particle that showed two drops and complete GFP signal loss shows a positive signal for CA (green) and Vpr (red), using nuclear staining with DAPI (blue) and cytoplasmic localization. (Scale bar: 100 nm.) (*C*) Mean intensity and signal-to-noise ratio of all live-imaged particles that were individually tracked. Groups were defined by their live-imaging GFP capsid integrity phenotype. Medians of the individual events are represented by gray bars, and interquartile ranges are shown as error bars. Open symbols show particles that challenged CD4 T cells, and red symbols show representative events measured from MDMs. (*D*) Three-dimensional SIM superresolution imaging of an MDM that was fixed after live imaging for 50 min. (Scale bar: 5 µm.) (*Inset*) Particle that showed two drops and complete GFP signal loss shows a positive signal for CA (green) and Vpr (red), using nuclear staining with DAPI (blue) and cytoplasmic localization. (Scale bar: 100 nm.) $*P < 0.5$; $***P < 0.01$.

that ultimately went on to infect a cell and begin producing Gag and budding virions. The observed infectious events in these infections at less than one particle per cell likely underrepresent the potential infected cells within the cultures due to length of observation time, cellular stress due to phototoxicity, and imperfect culture environment. In typical infectivity assays with reporter viruses, the experiments are run for 48 h to achieve maximal detection of infection. For these studies, we cultured the cells for up to 42 h, but often stopped earlier to preserve the observed cells for subsequent correlative analysis. Likewise, cellular state in the oxidative environment of phototoxicity and other cellular stresses of continuous imaging probably negatively impacted the cellular environment experienced by the virus. It is also difficult to translate the outcomes typically observed at the population level down to the limited observations at the individual cell level. The development of automated image analysis will allow the behavior of thousands of virions to be quantified to provide additional insights into the particle-to-infectivity ratio and the efficiency of the early steps of the HIV life cycle.

Another important consideration in interpreting the one particle per cell studies is the possibility of unlabeled viral particles that can be generated by the cotransfection of multiple plasmids. This issue is potentially relevant because single-particle analysis showed that the HIV-iGFP particle populations with different viral complex markers (Vpr or IN) or envelopes (pNL4-3 WT or VSV-G) tested here had 53–90% maturation in HIV-iGFP–labeled particles (Fig. S1). The viral preparations are generated by cotransfection of iGFP, a gag-pol expression vector, mCherryVpr, and VSV-G envelope, and, theoretically, unlabeled infectious particles could be present. In our experimental setting, only the viral RNA expressed from the HIV-Gag-iGFP plasmids contains LTRs, ensuring that infection will be reported by newly produced Gag-GFP fusion proteins. Therefore, under the conditions of virus production used here, it seems unlikely that particles could be produced which contain the iGFP genomic RNA but not the iGFP GFP-tagged Gag.

To validate this assumption, we performed RNA fluorescent in situ hybridization (FISH) targeting GFP, whose coding sequence is only present in the HIV-iGFP plasmid and genomic RNA (Fig. S1*I*). The analysis showed that ∼97% of the mature HIV particles ($AG3^+$) containing iGFP genomic RNA are GFP-labeled (Fig. S1 *G–I*), while the control HIV-iCherry particles that were produced in similar fashion to HIV-iGFP were negative for GFP containing RNA (Fig. S1 *G* and *I*). In contrast, only 0.6% of the GFP^- mature particles contain iGFP genomic RNA. This analysis reveals that there are no substantial populations of unlabeled viral particles that could confound the analysis connecting timing of capsid integrity loss and infectivity. Further supporting this viewpoint, we never observed any infected cells (GFP^+) that were not associated with iGFP-labeled particles, even under conditions where most cells never associated with a fluorescently labeled viral particle.

The HIV-iGFP construct allows the study of HIV-1 viral capsid status over time and the detection of the production of new viral particles that result from cell infection. The retention of cleaved GFP as a fluid phase marker inside of a virion and capsid uniquely allows detection of both the fusion event and subsequent loss of capsid integrity (Fig. 1 *A* and *B*). To address the possibility of GFP signal reduction in an acidic endosome in the case of VSV-G pseudotyping (43), we measured fusion directly with S15-tdTomato (Movie S2) and indirectly by the observation that after fusion, viruses are trapped in cytoplasmic TRIM bodies in the presence of MG132 (Fig. 2*B*). In recent years, several groups have discovered that it is possible to modulate "uncoating" of HIV-1 particles either by delaying or blocking reverse transcription, or by introducing certain mutations into the CA protein that forms the conical core (2, 23, 28, 29, 53, 54). A well-established mechanism to disrupt HIV capsid stability is to exploit the mechanism of TRIM5 restriction that recruits the proteasome to direct capsid disruption (16, 44). Specifically, TRIMCypA restriction can be modulated for the binding and disruption of the incoming viral capsid by the presence of the CsA washout assay. We used this ability to switch TRIMCypA restriction on and off to demonstrate that using the iGFP fluid phase marker validated the system presented here to monitor capsid integrity. In the absence of TRIMCypA function, thanks to the presence of CsA, we observed a median Δt (time between fusion and integrity loss) of ∼25 min (Fig. 2*B*). This result is in accordance with nonrestrictive infection. In an experimental setting where TRIMCypA can bind to the capsid but the proteasome-mediated capsid disruption is prevented by proteasome inhibitors, the HIV-iGFP capsids accumulate in an intact form within TRIMCypA bodies (Fig. 2*B*).

Because TRIMCypA requires an intact capsid to be able to bind and restrict HIV-1 infection, we have shown that the temporal measurement of GFP retention within the cone is a suitable method to measure capsid integrity. This timing is consistent with the CsA washout assay, which measured the time of loss of sensitivity to TRIM-CypA associated with virus infection (28), as well as with other systems that supported early changes in the integrity of the cone (16, 26, 27, 39, 55).

Recently, it was proposed that the ability of HIV-1 to escape cytoplasmic innate immunity is due to the shielding of the reverse-transcribed DNA by the viral capsid (9, 10). These studies showed that viral challenge to blood cells with a myeloid origin with the CA mutant N74D or P90A resulted in an antiviral state where the virus cannot replicate. This was interpreted as the activation of innate sensors by the prematurely exposed reverse-transcribing HIV genome. However, this hypothesis is not compatible with an early cytoplasmic uncoating, as demonstrated here, or with the demonstration that N74D uncoats with delayed kinetics. Here, we confirm that the N74D mutation leads to delayed uncoating (Fig. 2*A*), as originally revealed by the CsA washout assay (54). The observation that early uncoating is associated with infection calls for a reinterpretation of the mechanisms leading to the antiviral state described by Rasaiyaah et al. (10). Alternatively, it seems more likely that the induction of the antiviral state is caused by accumulation of dead-end reverse transcription products that could be more susceptible to innate recognition, especially at the high multiplicity of infection (MOI) used in such study. This possibility has recently been explored with another assay to detect capsid integrity in infected cells (56).

Here, we showed that HIV-iGFP capsid integrity can be sustained by the presence of NVP, a nonnucleoside reverse transcriptase inhibitor (Figs. 2*A* and 4). Strikingly, the removal of NVP from the live-imaging system results in a prompt loss of the integrity of the cone. The swift capsid integrity loss after resumption of reverse transcription supports a direct connection between uncoating and reverse transcription. The potential role of the interplay of reverse transcription and uncoating has been recently suggested to provide an enclosed environment facilitating first-strand transfer during HIV-1 reverse transcription (29). With the easy adaptability of our live-imaging fluorescence HIV-iGFP system, we tested this possibility in the transient presence of 7390, an RNase H activity inhibitor specific to HIV-1 reverse transcription (47) (Fig. 5*B*). The blocking of the RNase H-mediated degradation of the RNA template results in an inability of the newly synthesized ssDNA to anneal the complementary R region on the 3′ LTR RNA template during the first-strand transfer. Both in our live-imaging system and by using the CsA washout, we observed that the inhibition of RNase H activity delayed uncoating. The lack of an RNase H mutation to alter uncoating kinetics when monitored by DsRed-CypA tetramer labeling of the core remains a curious observation that raises questions related to the averaging of a large number of particles that do not lead to infection (27). We hypothesize that the contained environment of an intact capsid could be advantageous to the first-strand transfer between the DNA and RNA distinct and unlinked molecules. Within a constraining core, the two molecules would not diffuse away from each other. These data suggest that uncoating is delayed until first-strand transfer occurs, rather than the simple initiation of reverse transcription.

Historically, it has been suggested that uncoating kinetics might be distinct in different cell types or pathways leading to fusion. The flexibility of the HIV-iGFP live-imaging assay allows for testing under different experimental conditions, including different cell types and particles containing different envelope proteins. Importantly, we find that the general kinetics of uncoating are detectable ~30 min after fusion in the cell lines, primary $CD4^+$ T cells, and macrophages investigated here. Likewise, we find the same kinetics of uncoating with disparate envelopes, including X4 tropic HIV and VSV-G. Rather than cell type and entry pathway influencing uncoating, it appears that the efficiency of reverse transcription is more important (Figs. 2–4 and 6). However, it is not clear that this is how uncoating proceeds in other cell types. For example, it was recently reported that reverse transcription, nuclear localization, and loss of capsid took place at a slower rate in primary macrophages, as monitored by specific labeling of the viral DNA (38). Other circumstances in vivo may also show different kinetics of uncoating. For example, it was previously shown that virions can persist up to a week in the cytoplasm of peripheral blood mononuclear cells (PBMCs), and when the cells were activated, it resulted in viral growth out of the cultures (57, 58). That being said, most HIV replication studies are done in tissue culture systems similar to those used here and the presented results likely represent the series of events that takes place during the early phase of the HIV life cycle.

A big technical challenge to study uncoating was the ability to distinguish between integrity loss or a rearrangement of the capsid and the shedding of CA from the RTC. In this study, we observed a correlation between the loss of the GFP that is trapped within an intact core and a significant loss of CA that is present in the viral complex. This simultaneous loss of iGFP and reduction of the levels of CA, together with the observation that only early integrity loss of the capsid is associated with infection, allows us to describe uncoating as an early cytoplasmic process that is influenced by the first-strand transfer process of reverse transcription both in a cell line model and in primary cells that are known targets of HIV-1 (Figs. 5 and 6).

Critically, the "one-virus, one-cell" method pioneered here allowed us to identify that early uncoating is necessary for particle infectivity. The stochastic nature of infectivity and the unavoidable presence of defective particles have historically slowed progress in the field. We believe that this live-imaging system will be able to provide invaluable insight into host cofactor interactions with HIV, the cellular location and timing of specific events in HIV-1 infection, and innate sensor immunity at play. The ability to directly connect individual particle behavior through live-cell fluorescence microscopy to infectivity promises to bring clarity to our understanding of the early events of the HIV life cycle.

Materials and Methods

Cells. HEK-293T and CHOpgsa745 cells were cultured in DMEM, 10% FBS, L-glutamine, MEM nonessential amino acids solution (MEM-NEAA), and antibiotics. CHOpgsa745-TcypA cells were transduced and selected as reported before (59). $CD14^+$ cells were isolated from blood PBMCs with a Miltenyi Biotec MACS CD14 MicroBeads human kit (Fig. 4) or from blood with a StemCell Technologies EasySep Human Monocyte Isolation Kit (Fig. 6) following manufacturer instructions and differentiated to macrophages with macrophage colony-stimulating factor (M-CSF) (50 ng/mL), being washed every 2–3 d for 14 d preimaging. $CD4^+$ T cells were isolated from blood with a StemCell Technologies EasySep Human $CD4^+$ T-Cell Enrichment Kit and activated with CD3/CD28 antibodies 1 or 2 d before live imaging. MDMs and $CD4^+$ T cells were cultured in RPMI, 15% FBS, L-glutamine, and antibiotics. Stremlau cells were used in TRIM capture assays as previously reported (42).

Plasmids. HIV-Gag-iGFPΔEnv, HIV-Gag-iGFPWTEnv, HIV-N74DGag-iGFP-ΔEnv, and HIV-Gag-iCherryΔEnv full proviruses (with or without a point mutation in Env), which have a coding GFP in between the MA and CA proteins cleavage maturation sites in *gag* reading frame (41), are based in pNL4-3 HIV-1 plasmid. The psPAX2 was used as a Gag-Pol packaging vector that provided WT-Gag at a 1:1 ratio (Gag-iGFP/Gag-WT). Only HIV-Gag-iGFP plasmids contain LTRs. The pFSM-Gag plasmid was used for a tetracysteine motif suitable for ReAsH labeling (46). The pHIV-GFP (used for CsA washout) and pCMV–VSV-G were previously described (28). The pmCherry-Vpr and pGFP-Vpr were previously described (25, 42), and iRFP670Vpr plasmid was generated by replacing the mCherry sequence in pmCherry-Vpr by iRFP670 obtained from Addgene piRFP670-N1. The pLHA-owlTCypA-SN and pL57GPMoBeB sequences were previously described (59). The pGag-IN-mRuby was created by replacing GFP with the mRuby sequence; the original plasmid has been described elsewhere (36).

Virus Production. Viral particles were produced by polyethylenimine HEK-293T transfection, where DMEM medium was replaced 16 h posttransfection and viruses were collected 24 to 36 h posttransfection. HIV-iGFP-mCherryVpr viruses were produced by transfection with 3 μg of HIV-Gag-iGFP, 3 μg of psPAX2, 4 μg of pCMV–VSV-G, and 1.5 μg of mCherryVpr plasmids. ReASH-labeled viruses were produced by transfection with 3 μg of HIV-Gag-iGFP, 3 μg of pFSM-Gag, 4 μg of pCMV–VSV-G and 1.5 μg of iRFP670Vpr. HIV-iGFP and Gag-IN-mRuby

were produced by transfection with 5 μg of HIV-Gag-iGFP, 3 μg of pGag-IN-mRuby, and 4 μg of pCMV–VSV-G. Viruses transducing CHOpgsa745 cells to stably express HA-owlTRIMCypA were produced as previously reported (59).

Reagents. CsA was used at 5 μM; NVP was obtained from the NIH repository of the NIH AIDS Reagent Program, Division of AIDS, National Institute of Allergy and Infectious Diseases, NIH, and used at 10 μM (dissolved in water according to NIH AIDS Reagent Program solubility limit); MG132 was used at 1 μg/mL; Polybrene was used at 10 μg/mL; Oxyfluor/OxyRase was used at a 1:200 dilution; DL-lactate was used at 15 mM; and RnaseH inhibitor 7390 (shown as 8b in ref. 47) was used at 10 μM for live imaging and CsA washout experiments.

Western Blot Analysis. Viruses and whole-cell extracts were diluted with Laemmli buffer with β-mercaptoethanol, followed by boiling at 96 °C for 5 min, and loaded into precast Mini-PROTEAN TGX (5–20% gradient) gels. Nitrocellulose membranes were incubated with 1:1,000 241D antibody (NIH AIDS Reagent Program) and IRDye700 anti-human antibody. TRIM-CypA expression was measured with 3F10 (Roche) antibody and β-actin (Abcam), and with IRDye700 and IRDye800 secondary antibodies. Membranes were imaged with an Odyssey system.

ReAsH Labeling. HIV-iGFP-tetracysteine-CA-iRFP670Vpr (VSV-G) viruses were labeled for 2 h in a rotation chamber at 21 °C with TC-ReAsH II as described elsewhere (60, 61), replacing β-mercaptoethanol incubation with DTT (1 mM).

Flow Cytometry. Singlet cells (forward scatter (FSC)-height (H) by width (W) and side scatter (SSC) H by W) for the diverse mentioned infections were analyzed using a BD Fortessa FACS for the percentage of GFP signal using noninfected cells as a control. Controls to the infection level of one-particle, one-cell conditions (Fig. S1) were done under the same conditions as the imaged plates (detailed in *Live Imaging*) but maintained in a 37 °C 5% CO_2 incubator for 42 h. The cells in the plates (challenged with same amount of virus and viral incubation time, or without viruses) were detached with 250 μL of trypsin and fixed with 250 μL of fix solution (4:1 PBS/10% formaldehyde) before flow cytometry analysis.

CsA Washout Assay. CHOpgsa745-HA-owlTCypA cells were plated in 96-well dishes. Each experimental condition was performed in triplicate. Cells were spinoculated with HIV-GFP reporter virus and Polybrene for 1.5 h at 14 °C. Cells were washed with media at 37 °C and with CsA. CsA removal was done at different time points, as shown in Fig. 3*A* and Fig. S2*A*. As shown in Fig. 3*A*, the experiment was also exposed to RnaseH inhibitor 7390 incubation, in both the inoculation and first wash media. After 105 min, RnaseH inhibitor 7390 was removed from all reactions by replacement with warm media. Two days after infection, cells were detached with 50 μL of trypsin and fixed with 50 μL of fix solution (4:1 PBS/10% formaldehyde). The time of 50% uncoating was determined by curve fitting (28).

Live Imaging. A DeltaVision wide-field microscope (GE Life Sciences) equipped with an electron-multiplying charge-coupled device (EM CCD) camera, solid state illumination (SSI-LED) light path, or OMX DeltaVision Microscopy Imaging System (GE Life Sciences) equipped with complementary metal-oxide semiconductor (CMOS) cameras was used to acquire fluorescent values of HIV-iGFP viruses, tagged Vpr, or p24CA-ReaSH infecting cells plated in Delta T culture dishes. Cells were kept in a 37 °C heated chamber, together with a blood gas mixture (5% CO_2, 20% oxygen), throughout the imaging process. Oxyfluor and D-lactate were in solution with Fluorobrite DMEM (or RPMI without phenol red) with 20% FBS, L-glutamine, and MEM-NEAA. When used, NH_4Cl was used at a 10 mM concentration to synchronize infection from 20 to 45 min postvirus incubation. All VSV-G pseudotyped infections were done with Polybrene concentration of 5 μg/μL. Z-stacking spacing was set to 0.5 μm, with a total of 8- to 9-μm *z*-axis imaging. Experiments were done with the following emission conditions: GFP, 10% transmission and 50-ms exposure; mCherry, 10% transmission and 55-ms exposure (45 ms for Fig. 1 and 70 ms for Fig. 4); and brightfield, 32% transmission and 10-ms exposures (only a single Z in the middle of a cell is acquired for brightfield). Experiments illustrated in Fig. 5 were done with the following emission conditions: GFP, 32% transmission and 30-ms exposure; mCherry, 32% transmission and 40-ms exposure. When applicable, ReAsH imaging was performed at 10% transmission and 80-ms exposure, iRFP670Vpr was imaged at 32% transmission and 75-ms exposure, and IN-Ruby was imaged at 10% transmission 60-ms exposure. The number of experiments in each condition is detailed in *Statistics and Reproducibility*. Nominal magnification was 100× for all experiments with the exception of the one-particle, one-cell experiments, where a magnification of 60× was used to analyze a higher number of cells. $CD4^+$ T cells were immobilized to Delta T culture dishes coated for 30 min with Cell-TAK cell and tissue adhesive, according to manufacturer instructions.

Live Imaging Analysis. Z-stacks were deconvolved and z-projected using SoftWorx (GE Life Sciences) before individual mCherryVpr or iRFP670Vpr particle tracking over time using Imaris software (Bitplane). Mean intensities of HIV-iGFP or p24CA-ReAsH individual channels were analyzed by fitting discrete time points to a double-sigmoid equation with in-house–made Python scripts using scipy curvefit optimization, which uses the Levenberg–Marquardt algorithm (62). Centered particle video recordings were automatically generated by in-house–made Python scripts using matplotlib, with the data analyzed and exported from Imaris (63).

Fluorescence Kinetics Fitting. When analyzing fluorescence signal to estimate the timing of signal changes, it is important to avoid bias due to operator error. Data fitting provides reproducibility and precision. We therefore fit the fluorescence time series $I(t)$ in these experiments to the following heuristic double-sigmoidal form:

$$I(t) = \frac{I_{max} - I_{mid}}{2}\,\mathrm{erfc}(s_1(t - t_1)) + \frac{I_{mid} - I_{min}}{2}\,\mathrm{erfc}(s_2(t - t_2)) + I_{min},$$

where erfc(x) is the complementary error function, t_1 estimates the time of virus-cell fusion, and t_2 estimates the time of capsid integrity loss. We can then obtain the fusion-to-integrity-loss interval $\Delta t = t_1 - t_2$, which we plot in Figs. 1, 2, and 4. The final goodness of fit was estimated in Python/SciPy by calculating the Spearman correlation between the data and model. All Spearman correlations were greater than 0.8, with P values <0.00001.

Post–Time-Lapse Fixed Imaging. Live-imaged cells were washed with PBS and readily fixed with final 3.7% formaldehyde in piperazine-*N*,*N*′-bis (PIPES) buffer for 5 min, followed by three PBS washes. Cells were permeabilized for 10 min in block buffer (10% normal donkey serum, 0.01% NaN_3, 0.1% Triton X-100), followed by 241D and 71-31 mAbs (NIH AIDS Reagent Program) incubation at 1:1,000 for 1 h. The mAbs were washed three times with PBS and stained with anti-human AF647 antibodies (1:2,000) and DAPI (1:25,000) for 30 min. Secondary antibodies were washed three times with PBS and mounted overnight on 40-mm-radius coverslips with ProlongGold antifade. Cells were found using brightfield and iGFP/mCherryVpr virus references in the Deltavision microscope, followed by imaging in the superresolution 3D-SIM OMX DeltaVision Microscopy Imaging System. The synchronization of both microscopes' trays was used to find the correct cells and viral particles that were previously live-imaged. Mean intensities of particles were analyzed using ImageJ software (NIH) at the Z-slice that presented the highest p24CA staining signal for a given particle.

Virus on Glass. Viral preparations were spun on fibronectin-coated coverslips at 2,400 × *g* (90 min). Staining was performed with the same fixation and permeabilization as for cells (Fig. S1 *E* and *F*). In Fig. S1 *G*–*I*, Stellaris FISH Probes, using EGFP with Quasar 670 dye, were used following the protocol provided by the manufacturer (70% ethanol permeabilization for 1 h and hybridization with a probe concentration of 500 nM for 5 h).

Statistics and Reproducibility. Datasets in Fig. 1*D* were obtained from four independent experiments totaling 48 fields of view for the 2-h experiments (all events) and from four independent experiments totaling 400 fields of view for the >24-h experiments, where infection was directly linked to a single virion. All dual-drop data points were assumed nonnormal, and the Kruskal–Wallis test was performed (Fig. 2). The statistical null hypothesis showed a significant difference between different conditions by Kruskal–Wallis test rejection. The P values of Dunn's test of multiple comparisons for the different experiment conditions are then shown in the figures. The same analysis was performed for the dataset represented in Fig. 3*B* and 6*B* for the measurement of p24 intensities in the fixed samples. Each condition represents three independent experiments totaling 48 fields of view, 20 fields of view for the CD4 T-cell experiments, and 26 total fields of view for MDMs. To compare the simultaneous loss of GFP and ReAsH, and after performing data-fitting to the experimental data for each channel (as described in *Fluorescence Kinetics Fitting*), a nonparametric Spearman correlation coefficient and P value were calculated, as shown in Fig. 3*D*. The presented data were obtained from five independent experiments. In Fig. 4*B*, all data were assumed nonnormal, and a Mann–Whitney test was performed showing statistical significance between the datasets obtained from three independent experiments (48 fields of view) that are represented in the plot.

ACKNOWLEDGMENTS. We thank B. K. Chen for the HIV-iGFP construct and M. A. Parniak for the RnaseH inhibitor 7390. The following reagents were obtained through the NIH AIDS Reagent Program (Division of AIDS, National Institute of Allergy and Infectious Diseases, NIH): anti–HIV-1 p24 mAb (71-31, 241-D) from Dr. Susan Zolla-Pazner, mAb to HIV-1 p24 (AG3.0) from Dr. Jonathan Allan, and NVP. We thank R. T. D'Aquila and E. M. Campbell for critical review of this manuscript. We thank the James B. Pendleton Charitable Trust and the Third Coast Center for AIDS Research (CFAR) (P30 AI117943) for imaging equipment support. This work was supported by NIH Grant P50 GM082545 (subcontract to T.J.H.).

1. Ganser-Pornillos BK, Cheng A, Yeager M (2007) Structure of full-length HIV-1 CA: A model for the mature capsid lattice. *Cell* 131:70–79.
2. Forshey BM, von Schwedler U, Sundquist WI, Aiken C (2002) Formation of a human immunodeficiency virus type 1 core of optimal stability is crucial for viral replication. *J Virol* 76:5667–5677.
3. Schaller T, et al. (2011) HIV-1 capsid-cyclophilin interactions determine nuclear import pathway, integration targeting and replication efficiency. *PLoS Pathog* 7:e1002439.
4. Lee K, et al. (2010) Flexible use of nuclear import pathways by HIV-1. *Cell Host Microbe* 7:221–233.
5. Matreyek KA, Engelman A (2011) The requirement for nucleoporin NUP153 during human immunodeficiency virus type 1 infection is determined by the viral capsid. *J Virol* 85:7818–7827.
6. Brass AL, et al. (2008) Identification of host proteins required for HIV infection through a functional genomic screen. *Science* 319:921–926.
7. Marini B, et al. (2015) Nuclear architecture dictates HIV-1 integration site selection. *Nature* 521:227–231.
8. Lelek M, et al. (2015) Chromatin organization at the nuclear pore favours HIV replication. *Nat Commun* 6:6483.
9. Lahaye X, et al. (2013) The capsids of HIV-1 and HIV-2 determine immune detection of the viral cDNA by the innate sensor cGAS in dendritic cells. *Immunity* 39:1132–1142.
10. Rasaiyaah J, et al. (2013) HIV-1 evades innate immune recognition through specific cofactor recruitment. *Nature* 503:402–405.
11. Campbell EM, Hope TJ (2015) HIV-1 capsid: The multifaceted key player in HIV-1 infection. *Nat Rev Microbiol* 13:471–483.
12. Miller MD, Farnet CM, Bushman FD (1997) Human immunodeficiency virus type 1 preintegration complexes: Studies of organization and composition. *J Virol* 71:5382–5390.
13. Bukrinsky MI, et al. (1993) Association of integrase, matrix, and reverse transcriptase antigens of human immunodeficiency virus type 1 with viral nucleic acids following acute infection. *Proc Natl Acad Sci USA* 90:6125–6129.
14. Fassati A, Goff SP (2001) Characterization of intracellular reverse transcription complexes of human immunodeficiency virus type 1. *J Virol* 75:3626–3635.
15. Forshey BM, Shi J, Aiken C (2005) Structural requirements for recognition of the human immunodeficiency virus type 1 core during host restriction in owl monkey cells. *J Virol* 79:869–875.
16. Kutluay SB, Perez-Caballero D, Bieniasz PD (2013) Fates of retroviral core components during unrestricted and TRIM5-restricted infection. *PLoS Pathog* 9:e1003214.
17. Li Y-L, et al. (2016) Primate TRIM5 proteins form hexagonal nets on HIV-1 capsids. *eLife* 5:e16269.
18. Sayah DM, Sokolskaja E, Berthoux L, Luban J (2004) Cyclophilin A retrotransposition into TRIM5 explains owl monkey resistance to HIV-1. *Nature* 430:569–573.
19. Sebastian S, Luban J (2005) TRIM5alpha selectively binds a restriction-sensitive retroviral capsid. *Retrovirology* 2:40.
20. Shi J, Aiken C (2006) Saturation of TRIM5 alpha-mediated restriction of HIV-1 infection depends on the stability of the incoming viral capsid. *Virology* 350:493–500.
21. Stremlau M, et al. (2006) Specific recognition and accelerated uncoating of retroviral capsids by the TRIM5alpha restriction factor. *Proc Natl Acad Sci USA* 103:5514–5519.
22. Stremlau M, et al. (2004) The cytoplasmic body component TRIM5alpha restricts HIV-1 infection in old world monkeys. *Nature* 427:848–853.
23. Yang Y, Fricke T, Diaz-Griffero F (2013) Inhibition of reverse transcriptase activity increases stability of the HIV-1 core. *J Virol* 87:683–687.
24. Arhel NJ, et al. (2007) HIV-1 DNA Flap formation promotes uncoating of the preintegration complex at the nuclear pore. *EMBO J* 26:3025–3037.
25. McDonald D, et al. (2002) Visualization of the intracellular behavior of HIV in living cells. *J Cell Biol* 159:441–452.
26. Lukic Z, Dharan A, Fricke T, Diaz-Griffero F, Campbell EM (2014) HIV-1 uncoating is facilitated by dynein and kinesin 1. *J Virol* 88:13613–13625.
27. Francis AC, Marin M, Shi J, Aiken C, Melikyan GB (2016) Time-resolved imaging of single HIV-1 uncoating in vitro and in living cells. *PLoS Pathog* 12:e1005709.
28. Hulme AE, Perez O, Hope TJ (2011) Complementary assays reveal a relationship between HIV-1 uncoating and reverse transcription. *Proc Natl Acad Sci USA* 108: 9975–9980.
29. Cosnefroy O, Murray PJ, Bishop KN (2016) HIV-1 capsid uncoating initiates after the first strand transfer of reverse transcription. *Retrovirology* 13:58.
30. Dharan A, et al. (2016) KIF5B and Nup358 cooperatively mediate the nuclear import of HIV-1 during infection. *PLoS Pathog* 12:e1005700.
31. Jayappa KD, et al. (2015) Human immunodeficiency virus type 1 employs the cellular dynein light chain 1 protein for reverse transcription through interaction with its integrase protein. *J Virol* 89:3497–3511.
32. Malikov V, et al. (2015) HIV-1 capsids bind and exploit the kinesin-1 adaptor FEZ1 for inward movement to the nucleus. *Nat Commun* 6:6660.
33. Pawlica P, Berthoux L (2014) Cytoplasmic dynein promotes HIV-1 uncoating. *Viruses* 6: 4195–4211.
34. Sabo Y, et al. (2013) HIV-1 induces the formation of stable microtubules to enhance early infection. *Cell Host Microbe* 14:535–546.
35. Chin CR, et al. (2015) Direct visualization of HIV-1 replication intermediates shows that capsid and CPSF6 modulate HIV-1 intra-nuclear invasion and integration. *Cell Rep* 13:1717–1731.
36. Hulme AE, Kelley Z, Foley D, Hope TJ (2015) Complementary assays reveal a low level of CA associated with viral complexes in the nuclei of HIV-1-infected cells. *J Virol* 89:5350–5361.
37. Peng K, et al. (2014) Quantitative microscopy of functional HIV post-entry complexes reveals association of replication with the viral capsid. *eLife* 3:e04114.
38. Stultz RD, Cenker JJ, McDonald D (2017) Imaging HIV-1 genomic DNA from entry through productive infection. *J Virol* 91:e00034-17.
39. Xu H, et al. (2013) Evidence for biphasic uncoating during HIV-1 infection from a novel imaging assay. *Retrovirology* 10:70.
40. Rivière L, Darlix J-L, Cimarelli A (2010) Analysis of the viral elements required in the nuclear import of HIV-1 DNA. *J Virol* 84:729–739.
41. Hübner W, et al. (2007) Sequence of human immunodeficiency virus type 1 (HIV-1) Gag localization and oligomerization monitored with live confocal imaging of a replication-competent, fluorescently tagged HIV-1. *J Virol* 81:12596–12607.
42. Yu Z, et al. (2013) Unclosed HIV-1 capsids suggest a curled sheet model of assembly. *J Mol Biol* 425:112–123.
43. Padilla-Parra S, et al. (2013) Fusion of mature HIV-1 particles leads to complete release of a gag-GFP-based content marker and raises the intraviral pH. *PLoS One* 8:e71002.
44. Wu X, Anderson JL, Campbell EM, Joseph AM, Hope TJ (2006) Proteasome inhibitors uncouple rhesus TRIM5α restriction of HIV-1 reverse transcription and infection. *Proc Natl Acad Sci USA* 103:7465–7470.
45. Battivelli E, Lecossier D, Clavel F, Hance AJ (2013) Delaying reverse transcription does not increase sensitivity of HIV-1 to human TRIM5α. *PLoS One* 8:e52434.
46. Campbell EM, Perez O, Anderson JL, Hope TJ (2008) Visualization of a proteasome-independent intermediate during restriction of HIV-1 by rhesus TRIM5α. *J Cell Biol* 180:549–561.
47. Ilina T, Labarge K, Sarafianos SG, Ishima R, Parniak MA (2012) Inhibitors of HIV-1 reverse transcriptase-associated ribonuclease H activity. *Biology (Basel)* 1:521–541.
48. Arfi V, et al. (2008) Characterization of the early steps of infection of primary blood monocytes by human immunodeficiency virus type 1. *J Virol* 82:6557–6565.
49. Laguette N, et al. (2011) SAMHD1 is the dendritic- and myeloid-cell-specific HIV-1 restriction factor counteracted by Vpx. *Nature* 474:654–657.
50. Zhang H, et al. (1996) Kinetic analysis of intravirion reverse transcription in the blood plasma of human immunodeficiency virus type 1-infected individuals: Direct assessment of resistance to reverse transcriptase inhibitors in vivo. *J Virol* 70:628–634.
51. Thomas JA, Ott DE, Gorelick RJ (2007) Efficiency of human immunodeficiency virus type 1 postentry infection processes: Evidence against disproportionate numbers of defective virions. *J Virol* 81:4367–4370.
52. Butler SL, Hansen MS, Bushman FD (2001) A quantitative assay for HIV DNA integration in vivo. *Nat Med* 7:631–634.
53. Ambrose Z, et al. (2012) Human immunodeficiency virus type 1 capsid mutation N74D alters cyclophilin A dependence and impairs macrophage infection. *J Virol* 86:4708–4714.
54. Hulme AE, Kelley Z, Okocha EA, Hope TJ (2015) Identification of capsid mutations that alter the rate of HIV-1 uncoating in infected cells. *J Virol* 89:643–651.
55. Perez-Caballero D, Hatziioannou T, Zhang F, Cowan S, Bieniasz PD (2005) Restriction of human immunodeficiency virus type 1 by TRIM-CypA occurs with rapid kinetics and independently of cytoplasmic bodies, ubiquitin, and proteasome activity. *J Virol* 79: 15567–15572.
56. Da Silva Santos C, Tartour K, Cimarelli A (2016) A novel entry/uncoating assay reveals the presence of at least two species of viral capsids during synchronized HIV-1 infection. *PLoS Pathog* 12:e1005897.
57. Zack JA, et al. (1990) HIV-1 entry into quiescent primary lymphocytes: Molecular analysis reveals a labile, latent viral structure. *Cell* 61:213–222.
58. Zack JA, Haislip AM, Krogstad P, Chen IS (1992) Incompletely reverse-transcribed human immunodeficiency virus type 1 genomes in quiescent cells can function as intermediates in the retroviral life cycle. *J Virol* 66:1717–1725.
59. Mamede JI, Sitbon M, Battini J-L, Courgnaud V (2013) Heterogeneous susceptibility of circulating SIV isolate capsids to HIV-interacting factors. *Retrovirology* 10:77.
60. Lelek M, et al. (2012) Superresolution imaging of HIV in infected cells with FlAsH-PALM. *Proc Natl Acad Sci USA* 109:8564–8569.
61. Lelek M, Di Nunzio F, Zimmer C (2014) FlAsH-PALM: Super-resolution pointillist imaging with FlAsH-tetracysteine labeling. *Methods Mol Biol* 1174:183–193.
62. van der Walt S, Colbert SC, Varoquaux G (2011) The NumPy array: A structure for efficient numerical computation. *Comput Sci Eng* 13:22–30.
63. Hunter JD (2007) Matplotlib: A 2D graphics environment. *Comput Sci Eng* 9:90–95.